INTERNATIONAL JOURNAL FOR NUMERICAL AND ANALYTICAL METHODS IN GEOMECHANICS
Int. J. Numer. Anal. Meth. Geomech. 2014; **38**:370–390
Published online 19 July 2013 in Wiley Online Library (wileyonlinelibrary.com). DOI: 10.1002/nag.2211

A critical state sand plasticity model accounting for fabric evolution

Zhiwei Gao[1], Jidong Zhao[1,*,†], Xiang-Song Li[1] and Yannis F. Dafalias[2,3]

[1]*Department of Civil and Environmental Engineering, Hong Kong University of Science and Technology, Clearwater Bay, Kowloon, Hong Kong*
[2]*Department of Civil and Environmental Engineering, University of California, Davis, CA 95616, U.S.A.*
[3]*Department of Mechanics, School of Applied Mathematical and Physical Sciences, National Technical University of Athens, 15773, Athens, Greece*

SUMMARY

Fabric and its evolution need to be fully considered for effective modeling of the anisotropic behavior of cohesionless granular sand. In this study, a three-dimensional anisotropic model for granular material is proposed based on the anisotropic critical state theory recently proposed by Li & Dafalias [2012], in which the role of fabric evolution is highlighted. An explicit expression for the yield function is proposed in terms of the invariants and joint invariants of the normalized deviatoric stress ratio tensor and the deviatoric fabric tensor. A void-based fabric tensor that characterizes the average void size and its orientation of a granular assembly is employed in the model. Upon plastic loading, the material fabric is assumed to evolve continuously with its principal direction tending steadily towards the loading direction. A fabric evolution law is proposed to describe this behavior. With these considerations, a non-coaxial flow rule is naturally obtained. The model is shown to be capable of characterizing the complex anisotropic behavior of granular materials under monotonic loading conditions and meanwhile retains a relatively simple formulation for numerical implementation. The model predictions of typical behavior of both Toyoura sand and Fraser River sand compare well with experimental data. Copyright © 2013 John Wiley & Sons, Ltd.

Received 30 January 2013; Revised 14 May 2013; Accepted 12 June 2013

KEY WORDS: anisotropy; constitutive model; granular material; dilatancy; fabric evolution; critical state

1. INTRODUCTION

Due to gravitational deposition and/or compaction processes, naturally occurring materials such as sand often possess a transversely anisotropic fabric structure which greatly affects the strength and deformation characteristics of these materials and relevant geostructures, such as footings, foundations, embankment and dams. In investigating the bearing capacity of model strip foundations, for example, Azami *et al*. [1] have found that the difference in bearing capacity for one case with load being perpendicular to the bedding plane and the other with a parallel load can be up to 25%. There has been plenty of experimental evidence clearly indicating the key role of fabric anisotropy in contributing to the complex behavior of sand, such as strength, dilatancy and stiffness (see, e.g. [2–8]). This has partially fueled the great interest in the past few decades on theoretical characterization and modeling of fabric anisotropy in sand. Various approaches have been proposed to address the anisotropic sand behavior, e.g. those involving the use of rotated yield surface (see, e.g. [9–12]). However, yield surface rotation may not be able to account for the anisotropic nature of sand related to particle orientation, contact normal and void space distribution properly, as the magnitude and direction of rotation are typically associated with the initial stress state [13].

*Correspondence to: Jidong Zhao, Department of Civil and Environmental Engineering, Hong Kong University of Science and Technology, Clearwater Bay, Kowloon, Hong Kong.
†E-mail: jzhao@ust.hk

Meanwhile, the employment of fabric tensors derived from the microstructural information of sand has proved to be efficient in modeling sand behavior (e.g. [1, 14–23]). For simplicity, however, these studies have ignored the evolution of the fabric anisotropy during the deformation of the material. While such a simplified approach was successful to a certain extent for its purposes, it is also to an extent at odd with both experimental and numerical observations. In particular, as recently discussed by Li & Dafalias [24], ignoring the evolution of fabric anisotropy will inevitably lead to the loss of a unique critical state line – an intrinsic reference for a given soil established in the classical critical state soil mechanics.

The macroscopically observed sand behavior is in general a volumetric average of microstructural responses at particle level (e.g. [25–29]; see also [30]) and thus a fabric tensor at continuum level can be concretely linked to specific microstructural statistics. Recent microstructural studies with discrete element method (DEM) have shown that such a soil fabric tensor may experience significant changes in its magnitude and/or orientation during the loading course. Under sustained shear, the fabric tensor tends to become coaxial with the loading direction [28, 29] and an appropriately defined norm of the tensor approaches a constant. Based on these DEM observations and thermodynamics considerations, a critical state theory taking fabric anisotropy into account was proposed by Li & Dafalias [24], in which a unique critical state line is recovered.

In this paper, we shall develop a general rate-independent constitutive model for granular materials considering fabric anisotropy and its evolution, based on the aforementioned anisotropic critical state theory (ACST) by Li & Dafalias [24]. As entailed in the subsequent sections, the new model features an explicit yield function expressed in terms of the invariants and joint invariants of the stress ratio tensor r_{ij} and a deviatoric fabric tensor F_{ij} as well as a scalar internal variable H representing a characteristic shear resistance. Over a typical monotonic loading course, the fabric tensor is assumed to evolve towards the direction of loading. Based on the proposed framework, a non-coaxial flow rule is readily derived by which the non-coaxial behavior of stress and strain response can be explained in a natural way. Simulations by the model compare well with test results for Toyoura sand reported by Verdugo & Ishihara [31] and Yoshimine *et al*. [5] and for Fraser River sand by Uthayakumar & Vaid [7].

2. ANISOTROPIC SAND MODEL WITH FABRIC EVOLUTION

2.1. Yield function

Nemat-Nasser [32] studied the sliding along active shearing planes in a two-dimensional artificial granular packing and showed that the resistance to sliding is contributed from the isotropic Coulomb friction as well as the anisotropic distribution of contact normals. Based on this micromechanical deformation mechanism, we propose the following yield function,

$$f = \frac{R}{g(\theta)} - He^{-k_h(A-1)^2} = 0 \tag{1}$$

where $R = \sqrt{3/2 r_{ij} r_{ij}}$ with $r_{ij} = (\sigma_{ij} - p\delta_{ij})/p = s_{ij}/p$ being the stress ratio tensor, in which σ_{ij} is the stress tensor, $p = \sigma_{ii}/3$ is the mean normal stress, δ_{ij} is the Kronecker delta and s_{ij} is the deviator stress; H is a hardening parameter whose evolution law depends on the stress as well as internal variables including soil density and fabric; A is a fabric anisotropy variable; k_h is a non-negative model constant and $g(\theta)$ is an interpolation function based on the Lode angle θ of r_{ij} or s_{ij} as follows (personal communication, Z.L. Wang, 1992)

$$g(\theta) = \frac{\sqrt{(1+c^2)^2 + 4c(1-c^2)\sin 3\theta} - (1+c^2)}{2(1-c)\sin 3\theta} \tag{2}$$

where $c = M_e/M_c$, the ratio between the critical state stress ratio in triaxial extension M_e and that in triaxial compression M_c. It must be pointed out that the above yield function neglects for simplicity the plastic

DOI: 10.1002/nag

deformation under constant stress ratio r_{ij}. This simplification is in line with the scope of the present paper: highlighting only the new features concerning fabric anisotropy.

An important inclusion in the yield function in Eq. (1) is a fabric anisotropy variable A that is defined by the following joint invariant of the fabric tensor F_{ij} and the loading direction tensor n_{ij} (see also [19, 24, 33])

$$A = F_{ij} n_{ij} \tag{3}$$

where F_{ij} is a symmetric traceless tensor whose norm $F = \sqrt{F_{ij} F_{ij}}$ is referred to as the degree of fabric anisotropy. For convenience, F_{ij} is normalized such that in critical state, F is unity. For an initially cross-anisotropic sand sample with the isotropic plane (deposition plane) being the $x-y$ plane and deposition direction aligning with the z-axis, the initial F_{ij} can be expressed as

$$F_{ij} = \begin{pmatrix} F_z & 0 & 0 \\ 0 & F_x & 0 \\ 0 & 0 & F_y \end{pmatrix} = \sqrt{\frac{2}{3}} \begin{pmatrix} F_0 & 0 & 0 \\ 0 & -F_0/2 & 0 \\ 0 & 0 & -F_0/2 \end{pmatrix} \tag{4}$$

where F_0 is the initial degree of fabric anisotropy, i.e. the initial norm of F_{ij}. Note that in the above expression, a coordinate system aligned with the direction of sample deposition has been assumed. If one chooses a coordinate system which is not aligned with the deposition direction, a corresponding orthogonal transformation must be carried out. The *deviatoric unit loading direction tensor* n_{ij} in Eq. (3) is defined as follows [33]

$$n_{ij} = \frac{N_{ij} - N_{mn}\delta_{mn}\delta_{ij}/3}{\left\| N_{ij} - N_{mn}\delta_{mn}\delta_{ij}/3 \right\|} \tag{5}$$

with

$$N_{ij} = \frac{\partial \widetilde{f}}{\partial R}\frac{\partial R}{\partial r_{ij}} + \frac{\partial \widetilde{f}}{\partial g(\theta)}\frac{\partial g(\theta)}{\partial \theta}\frac{\partial \theta}{\partial r_{ij}} \tag{6}$$

where $\widetilde{f} = R/g(\theta)$. Obviously, $n_{ii} = 0$ and $n_{ij} n_{ij} = 1$. Notice that the n_{ij} is the deviatoric unit normal to a yield surface resulting from Eq. (1) with the assumption that A is a constant and not a function of stress as well (in other words, n_{ij} is not normal to the yield surface of Eq. (1)).

The yield function in Eq. (1) has been adopted based on the following considerations: (***a***) The first term in the equation, $R/g(\theta)$, is a normalized shear stress. While the second term, $He^{-k_h(A-1)^2}$, represents a generalized shear resistance, with H denoting a reference shear resistance – the shear resistance for $A = 1$. It follows that the actual shear resistance is the H modulated by the actual value of A via the term $e^{-k_h(A-1)^2}$. As A is a function of the fabric tensor F_{ij}, fabric anisotropy exerts an impact on the shear resistance. It is evident that, since k_h is positive, a larger A, i.e. a more intense fabric anisotropy in conjunction with more coaxial alignment between n_{ij} and F_{ij} will result in a higher shear resistance, in agreement with the observation by Nemat-Nasser [32]. Noticing that when $k_h = 0$, the yield function degenerates to a conventional isotropic yield surface in stress space. (***b***) At the *critical state*, according to the ACST [24], n_{ij} and F_{ij} become co-directional, and F reaches its critical state value 1. From Eq. (3), we have $A = 1$. As a result, the yield function in Eq. (1) becomes an isotropic critical state failure surface in the stress space which is identical to that proposed by Li & Dafalias [17]. An isotropic critical state failure surface independent of fabric anisotropy has its physical basis in both experimental and numerical observations [5, 34, 28] and is thermodynamically consistent as well. From a thermodynamics point of view, at critical state, the work input is completely dissipated so that there is no further development of frozen energy upon continuously developing shear deformation [35, 36]. It is to be emphasized that an isotropic failure surface at the critical state does not mean necessarily the critical state fabric is isotropic. This has been confirmed by recent DEM simulations as well (e.g. [29, 37, 38]).

DOI: 10.1002/nag

2.2. Elastic moduli and incremental elastic relation

As plastic strain dominates sand deformation, the influence of elastic anisotropy, if any, is considered negligible. The following isotropic pressure-sensitive elastic relations [17, 19, 24, 33, 39, 40] are employed:

$$G = G_0 \frac{(2.97 - e)^2}{1 + e} \sqrt{pp_a}, \qquad K = G \frac{2(1 + v)}{3(1 - 2v)} \tag{7}$$

where G and K denote the elastic shear and bulk modulus, respectively, G_0 is a material constant, e is the void ratio and v is the Poisson's ratio assumed to be a constant. In conjunction with Eq. (7), the following hypoelastic relation is assumed for calculating the incrementally reversible deviatoric and volumetric strain increments de^e_{ij} and $d\varepsilon^e_v$:

$$de^e_{ij} = \frac{ds_{ij}}{2G} \text{ and } d\varepsilon^e_v = \frac{dp}{K} \tag{8}$$

2.3. The elastoplastic stiffness tensor

Substituting Eq. (3) into Eq. (1) reveals that the proposed yield function includes two explicit internal variables: H and F_{ij}. Within the hypothesis that sand's stress–strain response is incrementally linear, the evolution of the two internal variables can be generally expressed as

$$dH = \langle L \rangle r_h \text{ and } dF_{ij} = \langle L \rangle \Theta_{ij} \tag{9}$$

where r_h and Θ_{ij} which are in general functions of the stress and internal variables including H and F_{ij} as well as others such as soil density represent the evolution direction for H and F_{ij}, respectively; L denotes the so-called plastic loading index, otherwise known as plastic multiplier; and $\langle\rangle$ are the Macauley brackets such that $\langle L \rangle = L$ for $L > 0$ and $\langle L \rangle = 0$ for any $L \le 0$.

The condition of consistency of the yield function (1) can now be written as follows:

$$\begin{aligned} df &= N_{ij} dr_{ij} + \frac{\partial f}{\partial H} dH + \frac{\partial f}{\partial A} dA = \left(N_{ij} dr_{ij} + \frac{\partial f}{\partial A} \frac{\partial A}{\partial n_{ij}} dn_{ij} \right) + \left(\frac{\partial f}{\partial H} dH + \frac{\partial f}{\partial A} \frac{\partial A}{\partial F_{ij}} dF_{ij} \right) \\ &= \left(N_{ij} + \frac{\partial f}{\partial A} \frac{\partial A}{\partial n_{kl}} \frac{\partial n_{kl}}{\partial r_{ij}} \right) dr_{ij} + \langle L \rangle \left(\frac{\partial f}{\partial H} r_h + \frac{\partial f}{\partial A} \frac{\partial A}{\partial F_{ij}} \Theta_{ij} \right) = 0 \end{aligned} \tag{10}$$

in which N_{ij} has been defined by Eq. (6). From Eq. (10), one has the loading index

$$L = \frac{1}{K_p} \left(N_{ij} + \frac{\partial f}{\partial A} \frac{\partial A}{\partial n_{kl}} \frac{\partial n_{kl}}{\partial r_{ij}} \right) dr_{ij} \tag{11}$$

where

$$K_p = -\left(\frac{\partial f}{\partial H} r_h + \frac{\partial f}{\partial A} \frac{\partial A}{\partial F_{ij}} \Theta_{ij} \right) \tag{12}$$

is the plastic modulus according to standard terminology in plasticity.

The plastic deviatoric strain increments de^p_{ij} can be written as $de^p_{ij} = \langle L \rangle m_{ij}$ where m_{ij} is a unit-norm deviatoric tensor containing only the information of the direction of de^p_{ij} and will be specified in the sequel. Based on the additive decomposition of the strain increment $d\varepsilon_{ij} = d\varepsilon^e_{ij} + d\varepsilon^p_{ij}$ into elastic

DOI: 10.1002/nag

and a plastic parts and the foregoing expression for the plastic strain increment, the loading index can also be expressed in terms of the total strain increment as

$$L=\underbrace{\frac{\left(N_{ij}+\frac{\partial f}{\partial A}\frac{\partial A}{\partial n_{kl}}\frac{\partial n_{kl}}{\partial r_{ij}}\right)\left[2G\left(\delta_{ip}\delta_{jq}-\frac{1}{3}\delta_{ij}\delta_{pq}\right)-Kr_{ij}\delta_{pq}\right]}{\left(N_{ij}+\frac{\partial f}{\partial A}\frac{\partial A}{\partial n_{kl}}\frac{\partial n_{kl}}{\partial r_{ij}}\right)\left(2Gm_{ij}-\sqrt{\frac{2}{3}}KDr_{ij}\right)+pK_p}}_{\Pi_{kl}}d\varepsilon_{pq}=\Pi_{kl}d\varepsilon_{kl} \tag{13}$$

in which

$$D=\frac{d\varepsilon_v^p}{d\varepsilon_q^p}=\frac{d\varepsilon_{ii}^p}{\sqrt{2de_{ij}^p de_{ij}^p/3}} \tag{14}$$

is the dilatancy. Using Eqs. (8) and (13), by standard procedure in plasticity, one obtains the incremental stress–strain relation

$$d\sigma_{ij}=\Lambda_{ijkl}d\varepsilon_{kl} \tag{15}$$

with the elastoplastic stiffness tensor

$$\Lambda_{ijkl}=K\delta_{ij}\delta_{kl}+2G\left(\delta_{ik}\delta_{jl}-\frac{1}{3}\delta_{ij}\delta_{kl}\right)-h(L)\left(2Gm_{ij}+\sqrt{\frac{2}{3}}KD\delta_{ij}\right)\Pi_{kl} \tag{16}$$

where $h(L)$ is the Heaviside step function, with $h(L>0)=1$ and $h(L\le 0)=0$.

2.4. Non-coaxial associated flow rule in the deviatoric space

It will be shown that a yield function like Eq. (1) including the joint invariant A naturally produces non-coaxial deformation for associated flow rule, i.e. the plastic strain rate tensor has different eigenvectors than those of the stress tensor.

The yield function Eq. (1) can be cast into the following general form:

$$f=\widetilde{f}\left(r_{ij},\mathrm{Z}_i\right)=0 \tag{17}$$

with Z_i denoting all scalar or tensor-valued internal variables; in the present model, the Z_i are H and F_{ij}.

By assuming an associated flow rule in the deviatoric stress space, the plastic deviatoric strain increments de_{ij}^p can now be written, as mentioned before Eq. (13):

$$de_{ij}^p=\langle L\rangle m_{ij},\ \text{ with }\ m_{ij}=\frac{\partial f/\partial r_{ij}-(\partial f/\partial r_{mn})\delta_{mn}\delta_{ij}/3}{\left\|\partial f/\partial r_{ij}-(\partial f/\partial r_{mn})\delta_{mn}\delta_{ij}/3\right\|} \tag{18}$$

Notice that m_{ij} is normal to the yield surface expressed by Eq. (1), unlike n_{ij} of Eq. (5) which is not. For the yield function Eq. (1), one has:

$$\frac{\partial f}{\partial r_{ij}}=\underbrace{\frac{\partial f}{\partial R}\frac{\partial R}{\partial r_{ij}}+\frac{\partial f}{\partial g(\theta)}\frac{\partial g(\theta)}{\partial(\theta)}\frac{\partial\theta}{\partial r_{ij}}}_{N_{ij}}+\frac{\partial f}{\partial A}\underbrace{\frac{\partial A}{\partial n_{kl}}}_{F_{kl}}\frac{\partial n_{kl}}{\partial r_{ij}}=N_{ij}+\frac{\partial f}{\partial A}F_{kl}\frac{\partial n_{kl}}{\partial r_{ij}} \tag{19}$$

A concrete derivation of the expression of $\partial f/\partial r_{ij}$ is given in the Appendix. Notably, the inclusion of fabric anisotropy via the joint invariant A in the yield function leads to $\partial f/\partial r_{ij}$ and m_{ij} consisting of two parts. The first part N_{ij} is obviously coaxial with the direction of the stress ratio r_{ij}, or equivalently the direction of the stress σ_{ij} itself; and the second part involving F_{kl} which is attributed to fabric

DOI: 10.1002/nag

anisotropy and is in general non-coaxial with r_{ij}. This feature naturally addresses the non-coaxiality issue in soil modeling. It is interesting to note that for a conventional model without consideration of fabric anisotropy, i.e. without the inclusion of A-dependent terms in the yield surface expression (1), the neutral stress path dictates $N_{ij}dr_{ij}=0$, on which no plastic deformation takes place. For the present model, however, as shown in Eq. (19), along such a path $(\partial f/\partial r_{ij})dr_{ij}=(\partial f/\partial A)F_{kl}(\partial n_{kl}/\partial r_{ij})dr_{ij}$, which is nonzero in general, rendering a plastic deformation containing non-coaxial components, which is in line with numerous experimental reports in the literature.

Nevertheless, the exact definition of neutral path loading is given by $(\partial f/\partial r_{ij})dr_{ij}=0$ and will yield no plastic strain rate at all. This also reveals one inherent weakness of this type of family of models with yield or loading surfaces that can expand isotropically and applies specifically to sands. During such neutral loading, which resembles but is not identical to the so-called rotational shear loading, it is shown experimentally that intense plastic deformations occur which cannot be predicted. To address this eventuality, additional loading mechanisms were introduced in Wang *et al.* [41] and Li & Dafalias [33], but such mechanisms will complicate the formulation and are not considered in this paper.

As observed by many researchers [5, 42], granular materials may exhibit an appreciable amount of deformation, which is non-coaxial with the stress during early stage of shearing. Such non-coaxiality, however, gradually diminishes when shearing proceeds to a high level. Indeed, from Eq. (19), we see that during non-proportional loading, the principal directions of r_{ij} and F_{ij} do not generally coincide, leading to a portion of plastic strain increment towards the direction of F_{ij} via the term $(\partial f/\partial A)F_{kl}(\partial n_{kl}/\partial r_{ij})$. As shearing proceeds, F_{ij} gradually evolves towards the loading direction [24], making the non-coaxial component smaller and smaller. Eventually, when critical state is approached at a very large strain level, F_{ij} becomes identical to n_{ij} resulting in $A=1$; hence, the last term of Eq. (1) equals H; consequently, $n_{ij}=m_{ij}$ and both are coaxial with r_{ij}. The evolution law of F_{ij} accounting for this fundamental feature will be addressed in a subsequent section in conjunction with a simple example of rotational shear to demonstrate this feature.

2.5. Dilatancy

The dilatancy as defined in Eq. (14) characterizes the volumetric response upon shearing, which is a unique feature of granular materials like soil. Eq. (14) indicates that the dilatancy defines the flow rule in the volumetric-deviator space, known to be non-associative. In other words, it does not have to be linked to the yield function.

Experimental and numerical evidence shows that the dilatancy of a granular material depends on its density, mean normal stress, fabric anisotropy, as well as the loading direction [5–7, 40, 28]. Manzari and Dafalias [43] and Li and Dafalias [40] have proposed a state-dependent dilatancy relation that considers the isotropic state parameter only. Li and Dafalias [17, 33] and Dafalias et al. [19] have included the effect of inherent (and not evolving) anisotropic fabric by modifying accordingly the location of the CSL in e-p space. In Li and Dafalias [24], the previous works were generalized to incorporate an evolving fabric tensor towards its critical state value, thus, introducing an anisotropic version of the state parameter and an ensuing unique CSL. In the present work, the dilatancy state parameter defined by Li & Dafalias [24] and associated formulation will be employed. We hereby propose the following fabric-dependent dilatancy function (c.f., [17, 24, 40]):

$$D=\frac{d_1}{M_c g(\theta)}\left[1+\frac{R}{M_c g(\theta)}\right][M_c g(\theta)\exp(m\zeta)-R] \tag{20}$$

where d_1 and m are two model constants. ζ is the dilatancy state parameter defined by Li & Dafalias [24]

$$\zeta=\psi-e_A(A-1) \tag{21}$$

where e_A is a model parameter. $\psi=e-e_c$ is the state parameter defined by Been and Jefferies [44] with e and e_c being the current void ratio and the critical state void ratio corresponding to the current

DOI: 10.1002/nag

mean normal stress p, respectively. In the present work, the critical state line in the $e-p$ plane is given by [45]

$$e_c = e_\Gamma - \lambda_c (p/p_a)^\xi \tag{22}$$

where e_Γ, λ_c and ξ are material constants and p_a (=101 kPa) is the atmospheric pressure. The relation expressed by Eq. (22) is found to be appropriate for modeling the critical state line of sand in the $e-p$ plane over a wide range of stress level [45]. It can also overcome some drawbacks of the commonly used $e-\ln p$ relation, i.e. the current relation gives $e_c = e_\Gamma$ at $p=0$ while the $e-\ln p$ relation gives an infinite value of e as p approaches 0.

2.6. Fabric evolution and plastic hardening

It remains practically difficult to quantify soil internal structure and its evolution by physical tests. Limited knowledge on such evolution has so far primarily been based upon micromechanics-based approaches such as DEM simulations (see, e.g. [28, 29, 37, 38, 46, 47]) and photoelastic experiments (e.g. [48]). Based on these as well as traditional macroscopic observations, the following evolution laws for H and F_{ij}, according to Li & Dafalias [24, 33], are proposed:

$$dH = \langle L \rangle r_h = \langle L \rangle \frac{G(1-c_h e)}{pR} [M_c g(\theta) \exp(-n\zeta) - R] \tag{23}$$

$$dF_{ij} = \langle L \rangle \Theta_{ij} = \langle L \rangle k_f \left(n_{ij} - F_{ij}\right) \tag{24}$$

where c_h and n are two positive model parameters; k_f is a new positive model constant representing the rate of fabric evolution. Note that the hardening law in Eq. (23) has been modified from the plastic modulus proposed by Li and Dafalias [17] with further inclusion of fabric anisotropy. The above evolution law of F_{ij} with plastic deformations leads towards coaxiality with the loading direction n_{ij}. Note that including additional terms involving plastic spin in Eq. (24) may help to address the mechanism of fabric rotation more realistically, as it has been discussed by Dafalias [49], Nemat-Nasser [32] and Li & Dafalias [24]. This will be investigated in a future work.

From Eq. (12) in conjunction with Eqs. (23) and (24), it follows that the expression for the plastic modulus is given by:

$$\begin{aligned} K_p &= \frac{R}{g(\theta)} \left[\frac{r_h}{H} + 2k_h (1-A) n_{ij} k_f \left(n_{ij} - F_{ij}\right) \right] \\ &= \frac{R}{g(\theta)} \left\{ \frac{G(1-c_h e)}{H} \left[\frac{M g(\theta) \exp(-n\zeta)}{R} - 1 \right] + 2k_h k_f (1-A)^2 \right\} \end{aligned} \tag{25}$$

As will be shown later, the plastic modulus may become negative to induce softening in dense samples under drained shear.

3. DATA SIMULATIONS BY THE MODEL

To verify the simulative capability of the present model, we employ the test data for the dry-deposited Toyoura sand ($G_s = 2.643$, $e_{\max} = 0.973$, $e_{\min} = 0.635$, $D_{50} = 0.17$mm) reported by Yoshimine *et al.* [5] and Verdugo & Ishihara [31] and those for the water-pluviated Fraser River sand ($G_s = 2.72$, $e_{\max} = 1.0$, $e_{\min} = 0.68$, $D_{50} = 0.3$mm) reported by Uthayakumar and Vaid [7] as well as Chillarige *et al.* [50]. These two groups of data can demonstrate the influence of confining pressure p_c, density denoted by D_{rc} which is the relative density after consolidation, intermediate principal stress parameter b as well

DOI: 10.1002/nag

as the major principal stress direction relative to the vertical direction α on undrained behavior of sand. All the model parameters are listed in Table I. The elastic parameters (G_0 and ν) and those related to the conventional critical state theory (M_c, c, e_Γ, λ_c and ξ) were calibrated based on the experimental data directly (see [40, 33, 51] for more detailed discussion), while other parameters were determined based on trial and error. However, it is noted that most of the model parameters are very close for these two sands, which is attributable to that their particle constitution, maximum and minimum void ratios are similar.

3.1. Dry-deposited Toyoura Sand

Figures 1 and 2 present two sets of undrained torsional shear test data with $b = 0.25$ and $b = 0.5$ for the dry-deposited Toyoura sand and the corresponding model simulations. The test setup and loading condition has been described by Yoshimine *et al*. [5] in detail. Clearly, the model well captures the trend that larger value of α generally leads to softer (lower shear stress $\sigma_1 - \sigma_3$ at the same shear strain $\varepsilon_1 - \varepsilon_3$) and relatively more contractive sand response. For both the $b = 0.25$ and $b = 0.5$ cases, the simulated shear stress–strain relations and effective stress paths are in good agreement with the test data when $\alpha \geq 30°$, while the model simulations are softer and more contractive than the measured when $\alpha \leq 15°$ (Figures 1 and 2). Better model performance can be obtained if r_h is further assumed to be dependent on A (see e.g. [24]) but additional parameter(s) will be needed. Meanwhile, it is interesting to have a further comparison of the performance of the present model with those proposed by Li & Dafalias [17] and Dafalias *et al*. [19] on the modeling of inherently anisotropic sand behavior. The predictions made in these two papers have been in excellent agreement with the test data of Toyoura sand as well. Nevertheless, the present model gives better performance in predicting the sand behavior at large strain levels with $\alpha > 45°$. While models in the two papers mentioned above predict an approximately linear $(\varepsilon_1 - \varepsilon_3) - (\sigma_1 - \sigma_3)$ relation after the 'quasi-steady state' in these cases, the current model captures the subtle nonlinear recovery of shear strength of sand behavior for this stage satisfactorily, due primarily to the consideration of the fabric evolution with the loading direction in our modeling.

3.2. Wet-tamped Toyoura sand

Figure 3 shows the experimental data and model simulations of wet-tamped Toyoura sand samples under drained triaxial compression conditions, with the same values of model constants in Table I

Table I. Summary of model parameters for dry-deposited Toyoura sand and water-pluviated Fraser River sand.

Parameter	Symbol	Toyoura sand	Fraser River sand
Elasticity	G_0	125	145
	ν	0.1	0.2
Critical state	M_c	1.25	1.33
	c	0.75	0.73
	e_Γ	0.934	1.021
	λ_c	0.02	0.03
	ξ	0.7	0.7
Yield function	k_h	0.03	0.03
Plastic modulus	c_h	0.90	0.90
	n	3.0	2.8
Dilatancy	d_1	0.2	0.15
	m	5.3	2.0
	e_A	0.10	0.11
Fabric evolution	k_f	5.7	5.8
Initial degree of anisotropy	F_0	0.45	0.45

DOI: 10.1002/nag

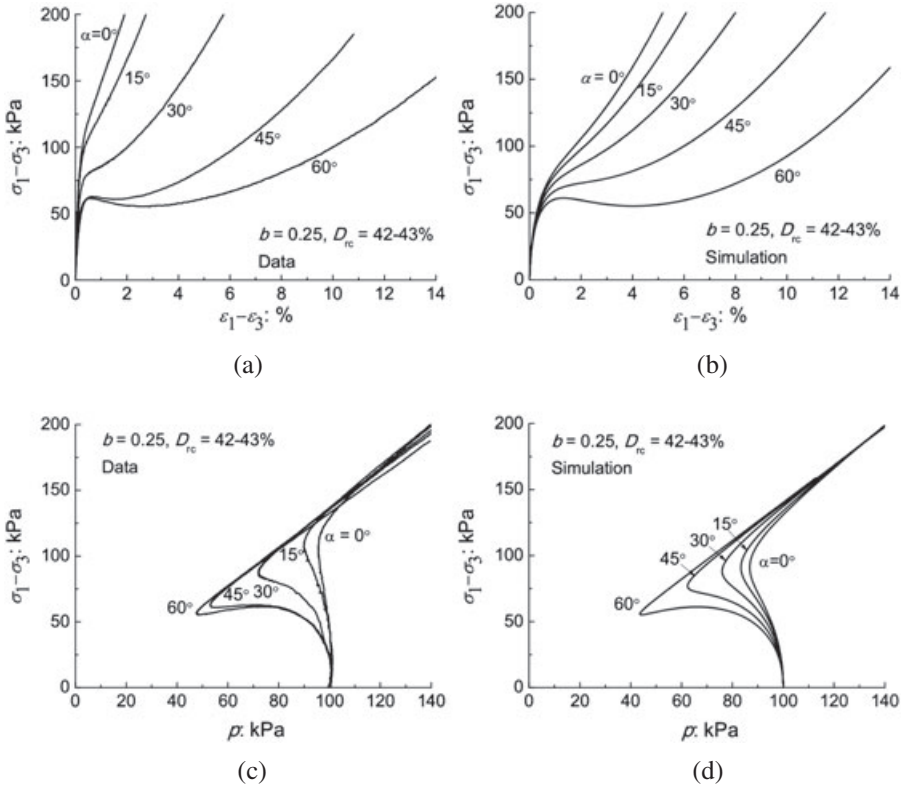

Figure 1. Test data and model simulations for the influence of principal stress direction α on undrained behavior of Toyoura sand at $b = 0.25$ (data from [5]).

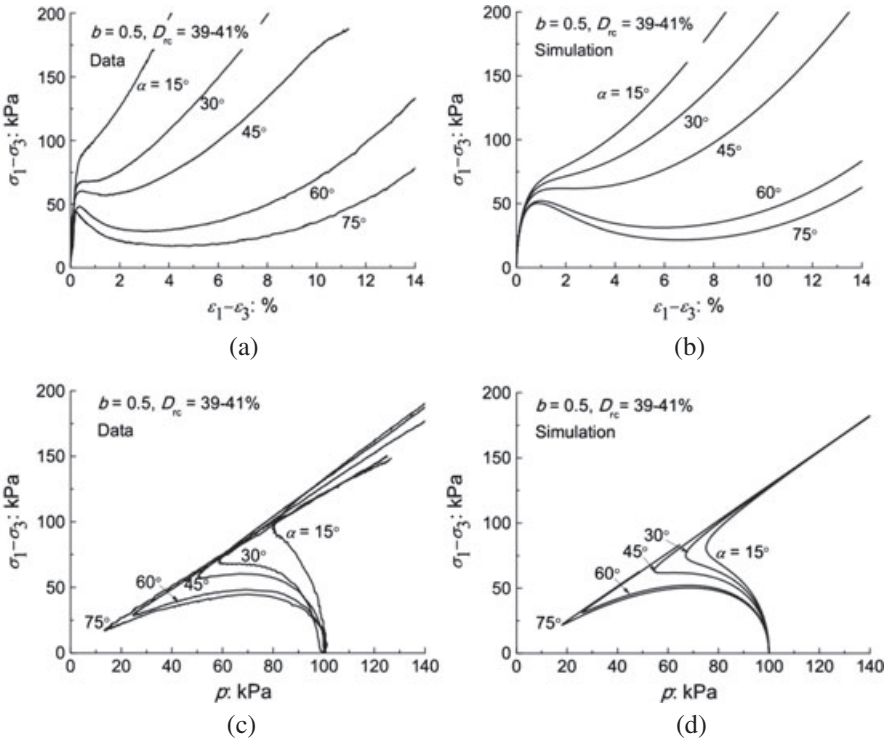

Figure 2. Test data and model simulations for influence of principal stress direction α on undrained behavior of Toyoura sand at $b = 0.5$ (data from [5]).

DOI: 10.1002/nag

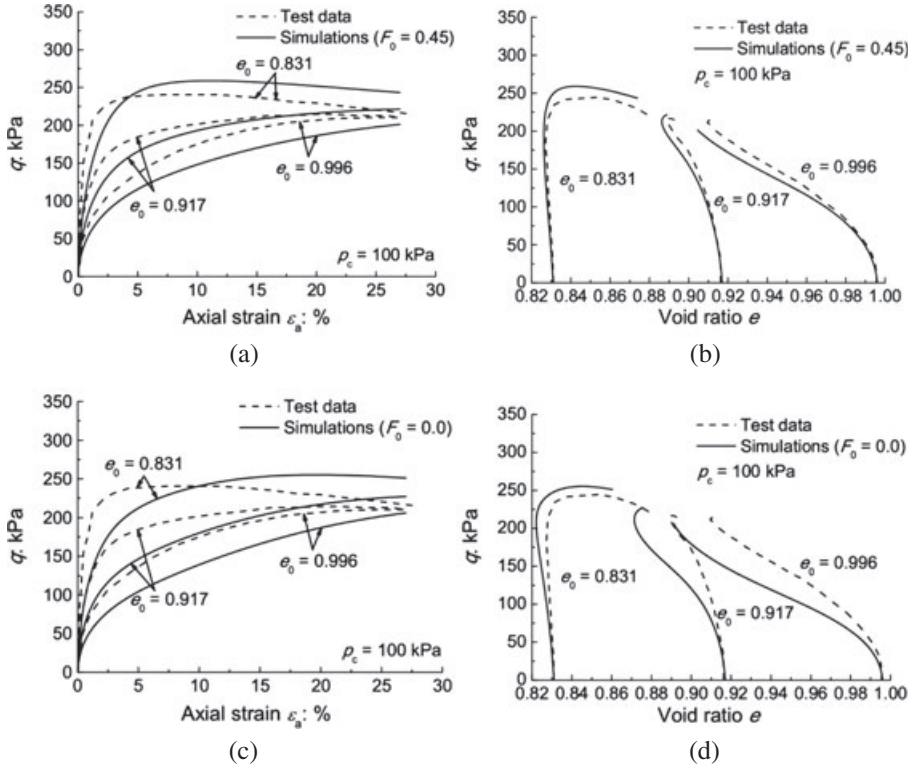

Figure 3. Test data and model simulations for the drained behavior of Toyoura sand under triaxial compression (data from [31]). Initial fabric anisotropy: (a) and (b): $F_0 = 0.45$; (c) and (d): $F_0 = 0.0$.

used for the undrained loading simulations for samples prepared by dry deposition. Despite the fact the samples were prepared now by a different method, which might induce a different initial fabric [52], the simulations in Figures 3(a) and (b) were conducted with an initial fabric norm value $F_0 = 0.45$ as in the undrained case of Figures 1 and 2 due to lack of any other information. Yet, the simulations are quite good if not as good as in the undrained case. In order to illustrate the important effect of initial fabric, Figures 3(c) and (d) show the same simulations using an initially isotropic fabric with $F_0 = 0.0$ while all other model constants are kept same. Since the fabric evolves towards the same critical state value, the differences between initially anisotropic and isotropic fabric values disappear as loading progresses, with the former providing a better overall simulation of the data.

3.3. Water-pluviated Fraser River sand

Comparisons of the model predictions with the test data for water-pluviated Fraser River sand in undrained torsional shear tests with constant b and α are presented in Figures 4, 5. Again, it is evident that the influences of loading direction, the intermediate principal stress level, the initial confining pressure as well as the relative density on the behavior of Fraser River sand as observed in the experiments by Uthayakumar & Vaid [7] are captured by our model. We notice that the gradual deviatoric stress increase after the 'quasi-steady state' with $\alpha \geq 45°$ is captured by the present model. Similar to the Toyoura sand case, the model gives better simulations when $\alpha \geq 45°$ (Figure 4) than other cases. Better model performance for cases with $\alpha \leq 30°$ can be achieved if r_h is assumed to be dependent on A.

4. FABRIC EVOLUTION EFFECTS ON SAND RESPONSE

We shall devote a detailed discussion in this section on the effect of fabric evolution on sand response under monotonic shear, as reflected from our modeling. In particular the discussion will be focused on

DOI: 10.1002/nag

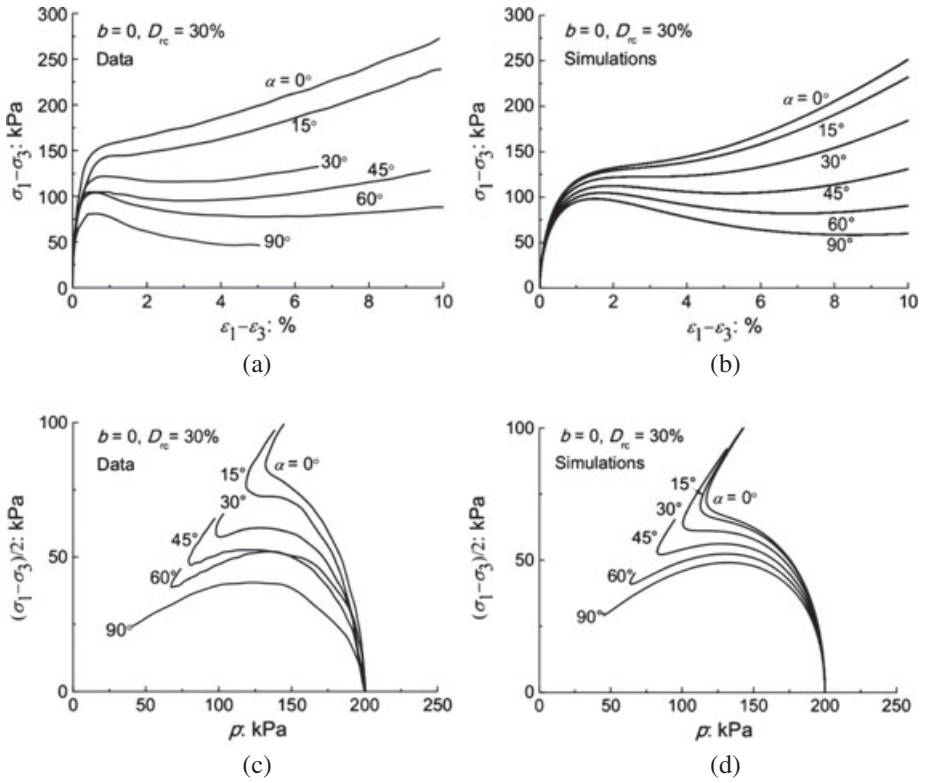

Figure 4. Undrained torsional shear test data and model simulations for effect of loading direction α on the behavior of Fraser River sand (data from [7]).

the effect of the evolution of the fabric norm and orientation on the anisotropic response, and on evolving and diminishing non-coaxiality of the plastic strain rate in regards to stress. In doing so, some additional simulations to the ones shown in the previous section will be exhibited.

4.1. Fabric evolution and anisotropy

Shown in Figure 6 are the model simulations of fabric evolution for Toyoura sand at $b = 0.5$. As can be seen from Figure 6(a) and (b), the critical state can be attained only at very high strain level (at about $\varepsilon_1 - \varepsilon_3 = 120\%$) when the sand fabric fully adapts to the stress orientation to form a steady anisotropic structure. Figures 6(a) and (b) are similar to Figures 6 and 7 in Li and Dafalias [24], showing this trend for a simplified triaxial model at $b = 0$ or $b = 1$ in triaxial compression and extension, respectively.

In more details, we observe from Figures 6(a) and (b) that A increases steadily with the strain over the loading course and reaches a unique critical state degree of anisotropy (fabric norm) $F = F_c = 1$ in all tests. It is also noticed that F decreases at the initial loading stage when $\alpha > 15°$ (Figure 6(b)) and subsequently increases towards its critical state value $F_c = 1$. This is because the fabric tensor F_{ij} evolves and changes its triaxial-like initial configuration, acquired during sample preparation, to the one of the applied stress at $b = 0.5$, and in the process its norm diminishes in order to accommodate this change; for the small angular deviation of $\alpha = 15^{\circ}$ such accommodation is not very strong. A particular case of this process has been observed in a triaxial extension test or a biaxial test by DEM with compression applied in the horizontal direction, as shown in Figure 6(d) (data from [28]). Note that the DEM samples were prepared to have an initially cross-anisotropic fabric similar to that of the real sand with horizontal bedding plane [28]. Under such loading conditions, the fabric tensor extracted from the DEM data is found to evolve from a triaxial compression-like structure towards a triaxial extension-like one. In such a process, the fabric norm first decreases to zero before it evolves towards its critical value of unity, while the principal directions of the fabric tensor do not change.

DOI: 10.1002/nag

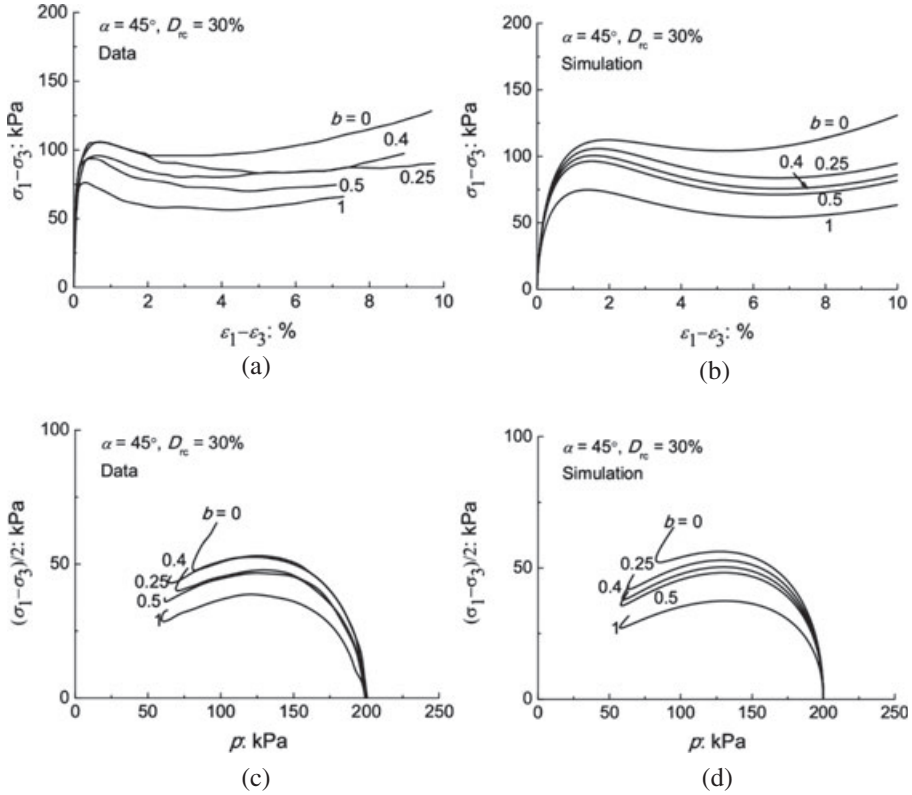

Figure 5. Test data and model simulations for the effect of intermediate principal stress ratio b on the behavior of Fraser River sand (data from [7]).

Such a special case of change in magnitude of fabric only can be regarded as a special case of fabric rotation (e.g. Figure 6(d)). Li and Dafalias [24] have also discussed this trend, where also a closed-form analytical solution of the fabric norm evolution was provided in Eq. (37) of the foregoing reference. In addition, as the fabric and the stress are non-coaxial at the beginning, the soil fabric must rotate its principal fabric axes to adjust its internal structure to sustain the external load more effectively. Under any circumstances, continuous loading and deformation will drive the fabric to continue to develop such that F retakes its increasing trend and approaches its critical state value at relatively large deformation (see also the DEM simulations in Figure 6(d)). These are the basic ingredients of the ACST postulated by Li and Dafalias [24]. Figure 6(c) shows the simulated relation between stress ratio R and A. For all the loading conditions, R first reaches a peak and then drops to the same critical state value while A keeps increasing. Same trend is also observed in the DEM simulations by Li and Yu [53].

Figure 7 shows similar simulations for drained loading. The same trend of initial increase and then decrease of the stress ratio R is observed, while the anisotropic variable A keeps increasing monotonically and the void ratio tends towards its critical state value for two loading orientations $\alpha = 0^0$ and $\alpha = 90^0$. A new interesting observation is made in Figure 7(c), which shows the evolution of the plastic modulus calculated from Eq. (25) and shows its variation from positive to negative and finally to zero values at critical state for the foregoing two orientations.

It is also interesting to have a closer look at the fabric evolution when static liquefaction occurs. Figure 8 shows the simulated responses of Toyoura sand under triaxial extension ($e = 0.866$) tests and the corresponding fabric evolution. This is in fact the case analyzed in Li and Dafalias [24] and briefly discussed in the previous paragraph, but it deserves special attention and additional discussion due to its importance and relevance to real experimental data. The fabric tensor is initially triaxial-compression like due to the sample's method of preparation; thus, it undergoes only a change of its norm, or

DOI: 10.1002/nag

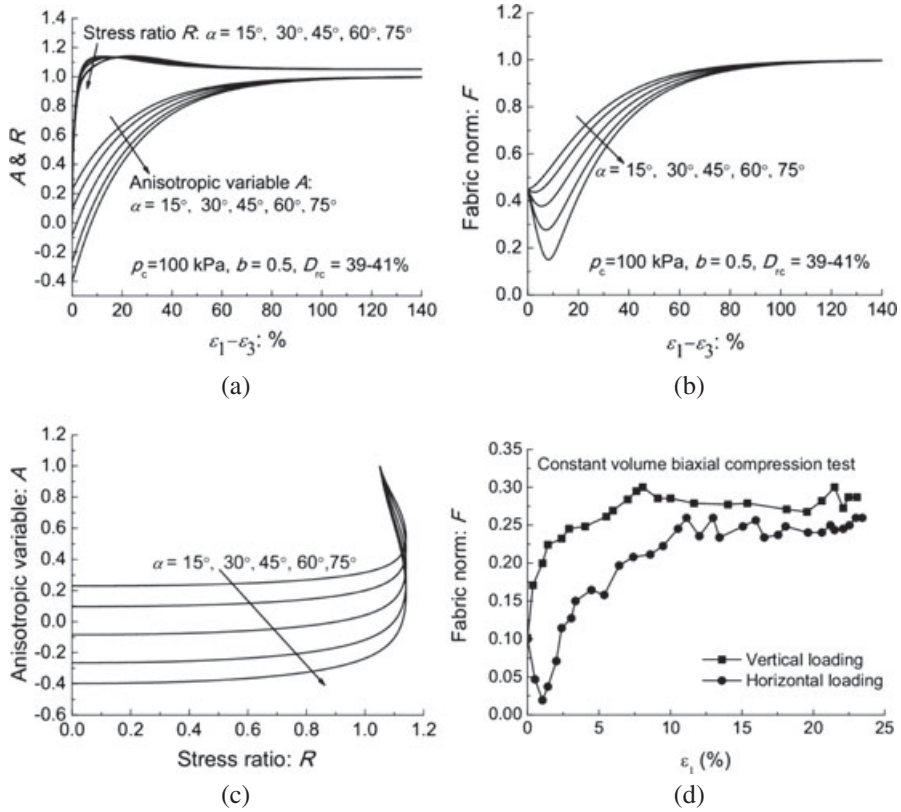

Figure 6. Model simulated fabric evolution for Toyoura sand under undrained shear at $b = 0.5$: (a) evolution of the anisotropic variable A and stress ratio R; (b) evolution of the degree of fabric anisotropy (fabric norm) F; (c) relation between R and A and (d) the simulated fabric evolution in biaxial compression tests by DEM (data from [28]).

equivalently of its principal values, without any change of its principal directions, which are the same with the applied load (triaxial compression and extension have same principal directions). In particular, the value of its major principal component decreases while the value of its minor principal component increases, which makes the norm F undergo a decrease first until at 7% deviatoric strain. At this point, all components of the fabric tensor are 0 so that a transient isotropic state is observed ($F = A = 0$). The above process continues with the increase of strain level. Eventually, the original minor component becomes the major one, whilst the original major one turns to be the minor one. The overall degree of anisotropy measured by F shows a slight rebound from zero (see Figure 8(c)). The discontinuity in the evolution of F does not influence the anisotropic variable A as A increases continuously from a negative value through zero to a positive one (Figure 8(c)). Nevertheless, both A and F reach a very small positive value at static liquefaction where $p = 0$, which is far smaller than their respective critical state value had liquefaction not occurred. Note that the aforementioned simulated results are in good agreement with the general trend observed from DEM simulations in Li [54] and with the corresponding results obtained by the closed-form solution for the evolution of F and A in Li and Dafalias [24] and shown in Figure 7 of the aforementioned reference. Figures 8(d) and (e) show the simulated stress path and fabric evolution in a biaxial compression test by DEM by Li [54] in which static liquefaction is observed. It can be seen that the degree of anisotropy F is around 0.16 when liquefaction occurs, which is about 59% of the critical state value (around 0.27 obtained from the DEM simulation). Note that the major principal stress direction is horizontal (the weakest or minor principal fabric direction of the material) in the DEM simulations (Figures 8(d) and (e)), which is similar to the triaxial extension loading condition in laboratory.

DOI: 10.1002/nag

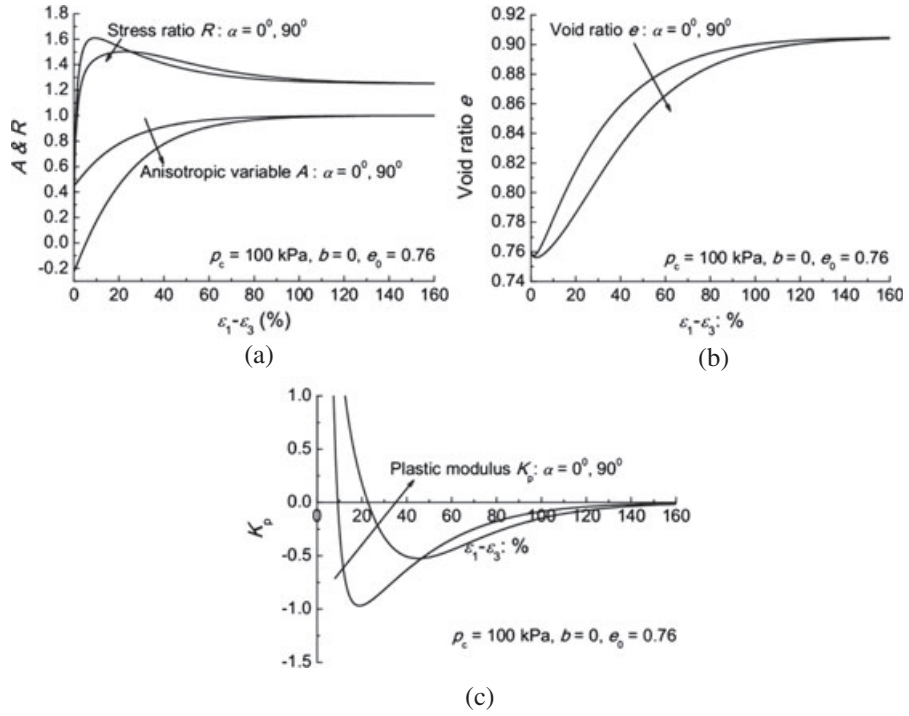

Figure 7. Model simulated evolutions of fabric and plastic modulus for Toyoura sand under drained triaxial compression: (a) evolution of the fabric anisotropic variable A and stress ratio R; (b) evolution of the void ratio; (c) evolution of the plastic modulus.

4.2. Fabric evolution and non-coaxiality

Another important feature of the present model is the non-coaxial flow rule in Eqs. (11)–(14), resulting naturally from the introduction of an evolving fabric tensor into the yield function and the associative flow rule assumption for the deviatoric plastic strain rate. As mentioned in Section 2.4, this flow rule may help to explain the non-coaxial behavior in sand. Indeed, while the soil fabric and the loading direction can be initially not coaxial to each other, the changes of stresses and the soil fabric are not always synchronized either. In a typical rotational shearing case, for example, the fabric will tend to align its major principal axes to be coaxial with that of the loading direction, in an attempt to reach an optimum internal rearrangement to bear the load. Nevertheless, the change of fabric is always lagging behind the stress change due to its passive nature, and this leads to non-coaxial stress and fabric tensor. According to the flow rule as presented in Eqs. (18)–(19), the plastic strain increment involves a component that does not align with the stress direction (the second term of the right-hand side of Eq. (19)), and consequently, the phenomenon of non-coaxiality may be handled with ease.

In a torsional shear test, the radial stress σ_r is always the intermediate principal stress and the radial strain ε_r the intermediate principal strain. In this setting, it is convenient to use our model to explain the non-coaxiality in the $z-\theta$ plane. To elaborate on this point and motivated by the approach in Dafalias *et al*. [19], we plot in Figure 9 the variation with shear strain of the difference of the angle $\alpha(\sigma)$ between the direction of the major principal stress σ_1 and the vertical direction, from the angle $\alpha(\varepsilon)$ that the major principal strain ε_1 forms with the vertical direction, for Toyoura sand under undrained shear. Such difference is a measure of non-coaxiality. The simulations match the experimental observation on non-coaxiality qualitatively well, and few remarks will help to improve our understandings. When $\alpha = 0°$ or $\alpha = 90°$, there is only change of the principal values of fabric tensor during the development of plastic strain, but no fabric rotation is involved. As such, the two sources of plastic strain increment due to stress and fabric increments will influence its value only, with its direction aligning with the stress direction during the entire loading course. Thus, the predicted sand response is generally coaxial, which is consistent with the experimental observation (see also [42]). In all the

DOI: 10.1002/nag

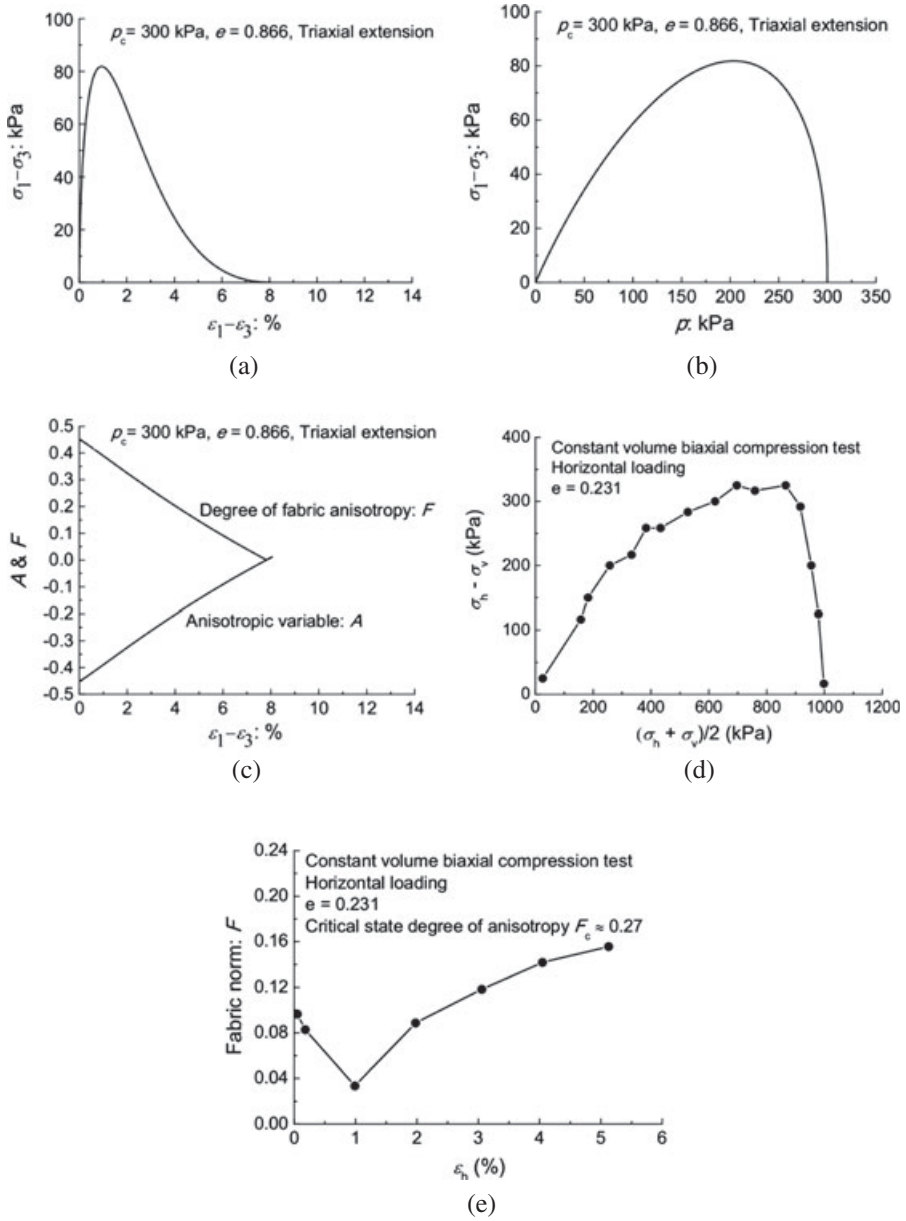

Figure 8. Model simulated fabric evolution for Toyoura sand in triaxial extension (c) wherein static liquefaction occurs ((a) and (b)) and DEM simulation of fabric evolution in biaxial compression tests (d) and (e) (data from [54]).

other cases, when α is between 0° and 90°, coaxiality is assumed for purely elastic stage (below 0.5% deviatoric strain) due to the employment of isotropic elastic relation in Eq. (7). Beyond this elastic stage to a relative low strain level (such as 2%), however, a distinct difference between $\alpha(\varepsilon)$ and $\alpha(\sigma)$ of the order of 4 to 5° on the average is found as shown in Figure 9, which indicates clearly non-coaxiality. The 4–5° of non-coaxiality after about 2% strain is not very significant from a practical perspective, but certainly it is important from a theoretical one. Upon further loading, the fabric tends to rotate towards the direction of stress, and the difference between $\alpha(\varepsilon)$ and $\alpha(\sigma)$ predicted by the model decreases after the peak, and the non-coaxiality will totally disappear at large strain levels. This was in fact the conclusion reached in Dafalias *et al*. [19] where the plots in their Figure 15, referred only to the residual values, in which case coaxiality was observed and modeled; the present approach shows the extent of the approximation made in the foregoing reference.

DOI: 10.1002/nag

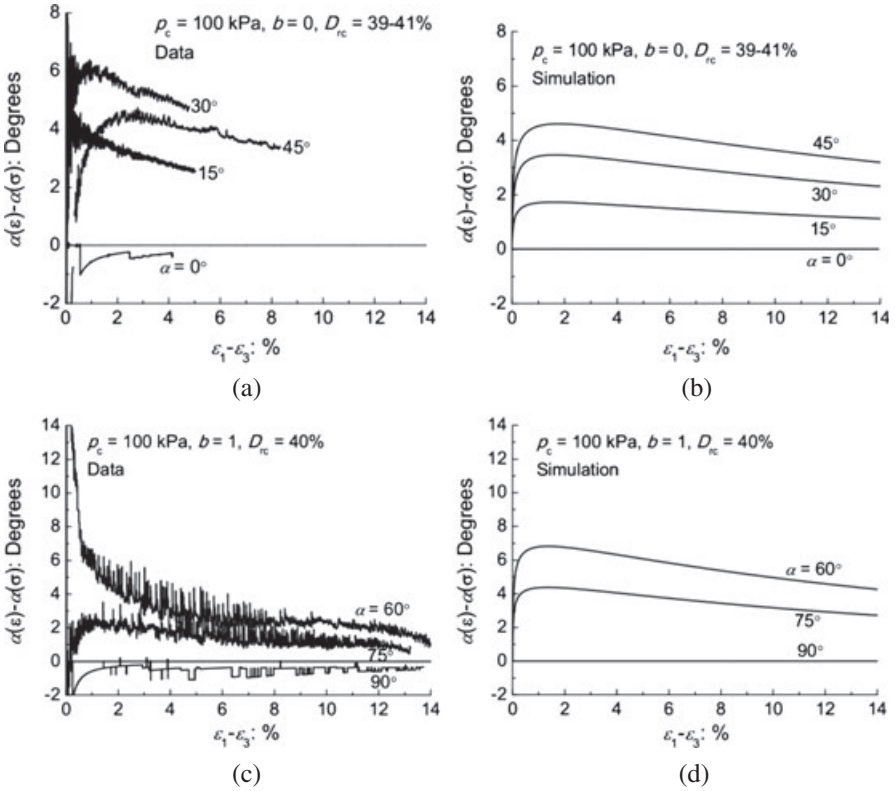

Figure 9. Test data and model simulations for the non-coaxial behavior of Toyoura sand under undrained rotational shear with (a), (b) $p_c = 100$ kPa, $b = 0$ and $D_{rc} = 39 - 41\%$ and (c), (d) $p_c = 100$ kPa, $b = 1$ and $D_{rc} = 40\%$.

Equivalent to the eventual disappearance of non-coaxiality is the reducing slope of the curves in Figure 9 after about 6% strain, which measures the non-coaxiality of the strain increment, rather than strain, in reference to the stress. However, it is observed that with $b = 0$ (Figures 9(a) and (b)), the present model predicts that the maximum difference is found in the case of $\alpha = 45°$, while the tests results show that this is attained when $\alpha = 30°$. This may be attributed to the possibility that the sand fabric in the tested samples is not rigorously cross-anisotropic at the initial state. Nevertheless, the current model captures the general trend of $\alpha(\boldsymbol{\varepsilon}) > \alpha(\boldsymbol{\sigma})$ which is frequently observed in sand [5]. Meanwhile, it is emphasized that improved modeling on the rotational shear can be achievable by including the plastic spin effect in the fabric evolution law in Eq. (20) as shown in Li and Dafalias [24], and this will be investigated in a future work.

Intimately related to non-coaxiality is the shape of the yield surface and associated neutral loading path tangentially to it (in fact the yield surface shape is the neutral loading path), since the assumed associative flow rule will depend on such shape in the deviatoric stress space. Hence, with Figure 10(a) illustrating the relative orientation of stress and fabric tensor in terms of their principal directions and angle α, Figure 10(b) shows the shape of the yield surface as given by Eq. (1) and plotted in the deviatoric π-plane of the stress ratio space, for three cases as indicated in the figure caption. Comparing cases 1 and 2, one can see a small variation in shape but mainly a change of size; this is due to the dependence of the 'size' of f on A (last term in Eq. (1)), and A depends on the norm and the relative orientation of fabric and loading direction; then, while the norm is same (same F_0) for cases 1 and 2, the relative orientation is different due to different α, hence different values of A arise. Comparison now of cases 2 and 3 shows the effect of fabric anisotropy on the shape of the yield surfaces, in particular between the isotropic fabric for $F_0 = A = 0$ and an anisotropic fabric for $F_0 = 0.9$ at $\alpha = 45^0$. Observe the normal 'tensors' to each one of the two yield surfaces, shown by small arrows at their intersection point; the difference of these two normal directions is a graphical measure of

DOI: 10.1002/nag

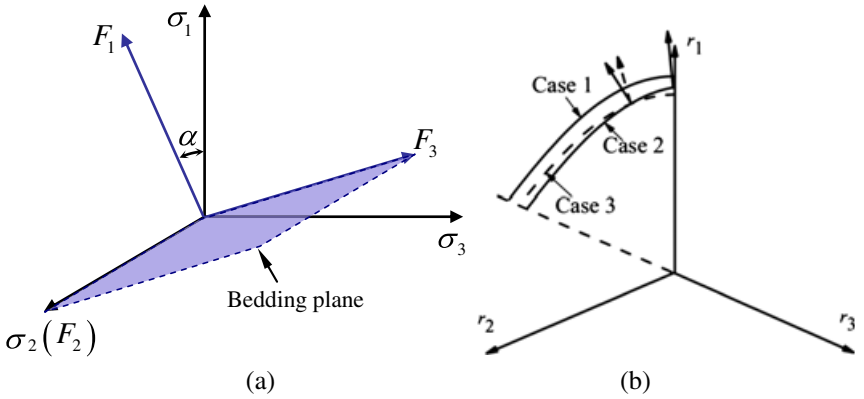

Figure 10. Demonstration of yield surface shapes and associated neutral loading paths for the current model for Toyoura sand for three cases: Case 1: $\alpha = 0°$ degree of anisotropy: $F_0 = 0.9$; Case 2: $\alpha = 45°$, degree of anisotropy: $F_0 = 0.9$; Case 3: $F_0 = 0.0$; Isotropic fabric case, $A \equiv 0$. (a) Definition of α; (b) the obtained yield surface shapes (neutral loading paths).

non-coaxiality because the normal for the isotropic case 3 will be coaxial with the stress, while the normal for the anisotropic case 2 will not.

Another result of anisotropy and resulting non-coaxiality can be seen if one observes what happens at the intersection points of the three yield surfaces with the axis r_1 in Figure 10(b). For cases 1 and 3, the normal to the yield surface at the corresponding intersection point with axis r_1 (not shown for clarity) is parallel to the axis indicating coaxiality, which for case 1 is the result of $\alpha = 0$ (fabric tensor and stress are coaxial) while for the case 3 is simply the result of isotropy. However, it is clear from the plot of Figure 10(b) that the corresponding normal for case 2 will deviate from axis r_1, and such deviation is a measure of non-coaxiality because of anisotropic fabric tensor being non-coaxial with the stress tensor even at the triaxial compression state which exists on axis r_1.

5. CONCLUDING REMARKS

A three-dimensional elastoplastic constitutive model has been proposed to describe the anisotropic behavior of sand. The model is characterized by the following key features:

1. It is constructed within the framework of ACST recently presented by Li and Dafalias [24]. Being a totally new theory different from the classic one, the ACST emphasizes the role of fabric on the characterization of sand response at critical state. It states that Critical State is reached when in addition to critical values for the stress and void ratios, the soil fabric must also reach a critical state value properly associated with a loading direction.
2. It employs a void-based fabric tensor and a physically based fabric evolution law to account for the influence of void sizes and orientations and their change during shear on the sand behavior, dilatancy in particular. To the knowledge of the authors, no previous soil model had ever incorporated a fabric tensor evolving towards a unique critical state value. The physical significance of the fabric evolution law is that the fabric will evolve to accommodate the applied stress and increase the sand resistance to shear during the loading process, as well as the impact on the soil dilatancy and plastic hardening.
3. It introduces an explicit anisotropic yield function expressed by the direct and joint isotropic invariants of the stress tensor and fabric tensor, on the physical basis that the shearing resistance of the soil consists of contributions from the isotropic inter-particle friction and the fabric anisotropy, and that the dissipation rate is dependent on the soil fabric.
4. A non-coaxial but associative flow rule in the deviatoric stress space that can naturally account for the non-coaxial behavior of initially anisotropic sand samples under monotonic loading is employed, in regards to a yield surface – plastic potential that includes joint invariants of stress and fabric tensors. Such a non-coaxial flow rule helps to explain the physical mechanism underlying

DOI: 10.1002/nag

the non-coaxial behavior in sand in a natural yet reasonable way, rather than being arbitrary and phenomenological as in many existing studies. Evidently, the employment of a fabric-dependent flow rule and consideration of fabric evolution with plastic deformation is emphatically important for modeling the transition of sand response from being non-coaxial at the beginning of loading when the fabric and stress are notably non-coaxial to being coaxial at critical state when the fabric is co-directional with loading. Never has this feature been reported in the existing studies.

The model has been used to simulate a series of undrained test results for the dry-deposited Toyoura sand [5] and water-pluviated Fraser River sand [7], as well as drained test for moist-tamped Toyoura sand [31], under various combinations of principal stress directions, intermediate principal stress values, confining pressure and densities. The model simulations compare well with the test results under different loading paths with a single set of parameters. The new model demonstrates excellent predictive capabilities in capturing such complex behaviors of sand as phase transformation, static liquefaction as well as critical state. It is emphasized that the evolution of fabric anisotropy is a natural process and plays a key role behind the complex behavior of sand, and should be carefully considered in the modeling of sand in the future. Future work will be focused on modeling the behavior of sand under more complex loading conditions, which are of important engineering significance, such as reverse loading and principal stress rotation.

NOTATION

A	anisotropic variable
b	intermediate principal stress parameter
D	dilatancy equation
D_{rc}	relative density after consolidation
e, e_c	void ratio and critical state void ratio
e_{ij}	deviatoric strain
e^e_{ij}, e^p_{ij}	elastic and plastic deviatoric strain
F_{ij}	deviatoric void fabric tensor
f	yield function
G	elastic shear modulus
H	hardening parameter
$g(\theta)$	interpolation function for the critical state stress ratio
K	elastic bulk modulus
K_p	plastic modulus
M_c, M_e	critical state stress ratio in triaxial compression and triaxial extension
p	mean stress
p_c	consolidation pressure before shear
R	stress ratio
r_{ij}	stress ratio tensor
s_{ij}	deviatoric stress tensor
α	angle between the major principal stress and direction of deposition
δ_{ij}	Kronecker delta
ε_1, ε_2, ε_3	major, intermediate and minor principal strain respectively
ε_q, ε^e_q, ε^p_q	total, elastic and plastic deviatoric strain respectively
ε_r	radial strain
ε_v, ε^e_v, ε^p_v	total, elastic and plastic volumetric strain, respectively
ε_z	vertical strain
θ	Lode angle of the stress tensor
v	Poisson's ratio
σ_1, σ_2, σ_3	major, intermediate and minor principal stress, respectively
σ_{ij}	stress tensor
σ_r, σ_z	radial and vertical stress
ψ	state parameter

DOI: 10.1002/nag

APPENDIX. PARTIAL DERIVATIVES USED IN THE CONSTITUTIVE RELATION

The expression for $\frac{\partial f}{\partial r_{ij}}$ can be obtained according to the chain rule for partial derivatives based on Eq. (1),

$$\frac{\partial f}{\partial r_{ij}} = \frac{\partial f}{\partial R}\frac{\partial R}{\partial r_{ij}} + \frac{\partial f}{\partial \theta}\frac{\partial \theta}{\partial r_{ij}} + \frac{\partial f}{\partial A}\frac{\partial A}{\partial n_{kl}}\frac{\partial n_{kl}}{\partial r_{ij}} = N_{ij} + \frac{\partial f}{\partial A}\frac{\partial A}{\partial n_{kl}}\frac{\partial n_{kl}}{\partial r_{ij}} \tag{A1}$$

where

$$\begin{aligned} N_{ij} &= \frac{\partial \widetilde{f}}{\partial r_{ij}} = \frac{1}{g(\theta)}\frac{\partial R}{\partial r_{ij}} - \frac{R}{g^2(\theta)}\frac{\partial g(\theta)}{\partial \theta}\frac{\partial \theta}{\partial r_{ij}} \\ &= \frac{3}{2R^2 g^2(\theta)}\left\{\left[Rg(\theta) + 3R\sin 3\theta \frac{\partial g(\theta)}{\partial \sin 3\theta}\right] r_{ij} + 9\frac{\partial g(\theta)}{\partial \sin 3\theta} r_{im} r_{jm}\right\} \end{aligned} \tag{A2}$$

$$\frac{\partial f}{\partial A} = 2k_h H(A-1)e^{-k_h(A-1)^2}, \quad \frac{\partial f}{\partial F_{ij}} = \frac{\partial f}{\partial A}\frac{\partial A}{\partial F_{ij}}, \quad \frac{\partial A}{\partial n_{ij}} = F_{ij}, \quad \frac{\partial A}{\partial F_{ij}} = n_{ij} \tag{A3}$$

$$\begin{aligned} \frac{\partial n_{ij}}{\partial r_{kl}} &= \frac{3}{4Rg(\theta)}\left(1 + \frac{3\sin 3\theta\, \partial g(\theta)}{g(\theta)\ \partial \sin 3\theta}\right)\left(\delta_{ik}\delta_{jl} + \delta_{il}\delta_{jk}\right) \\ &+ \frac{27}{4R^2 g^2(\theta)}\frac{\partial g(\theta)}{\partial \sin 3\theta}\left(r_{ik}\delta_{jl} + r_{il}\delta_{jk} + r_{lj}\delta_{ik} + r_{kj}\delta_{il}\right) \\ &+ \frac{9}{4R^3 g(\theta)}\left\{-1 + \frac{9\sin 3\theta}{g(\theta)}\left[\frac{2\sin 3\theta}{g(\theta)}\left(\frac{\partial g(\theta)}{\partial \sin 3\theta}\right)^2 - \frac{\partial g(\theta)}{\partial \sin 3\theta} - \sin 3\theta \frac{\partial^2 g(\theta)}{\partial(\sin 3\theta)^2}\right]\right\}\left(r_{ij}r_{kl}\right) \\ &+ \frac{81}{4R^4 g^2(\theta)}\left[\frac{6\sin 3\theta}{g(\theta)}\left(\frac{\partial g(\theta)}{\partial \sin 3\theta}\right)^2 - 2\frac{\partial g(\theta)}{\partial \sin 3\theta} - 3\sin 3\theta \frac{\partial^2 g(\theta)}{\partial(\sin 3\theta)^2}\right]\left(r_{ij}r_{kp}r_{pl} + r_{ip}r_{pj}r_{kl}\right) \\ &+ \frac{729}{4R^5 g^3(\theta)}\left[2\left(\frac{\partial g(\theta)}{\partial \sin 3\theta}\right)^2 - g(\theta)\frac{\partial^2 g(\theta)}{\partial(\sin 3\theta)^2}\right] r_{kp}r_{pl}r_{iq}r_{qj} \\ &- \frac{27\sin 3\theta}{2R^2 g^2(\theta)}\left[\frac{2}{g(\theta)}\left(\frac{\partial g(\theta)}{\partial \sin 3\theta}\right)^2 - \frac{\partial^2 g(\theta)}{\partial(\sin 3\theta)^2}\right]\delta_{ij}r_{kl} \\ &- \frac{81}{2R^3 g^2(\theta)}\left[\frac{2}{g(\theta)}\left(\frac{\partial g(\theta)}{\partial \sin 3\theta}\right)^2 - \frac{\partial^2 g(\theta)}{\partial(\sin 3\theta)^2}\right]\delta_{ij}r_{kp}r_{pl} \end{aligned} \tag{A4}$$

with

$$\frac{\partial g(\theta)}{\partial \sin 3\theta} = \frac{c(1+c)}{\sin 3\theta\sqrt{(1+c^2)^2 + 4c(1-c^2)\sin 3\theta}} - \frac{g(\theta)}{\sin 3\theta} \tag{A5}$$

and

$$\frac{\partial^2 g}{\partial(\sin 3\theta)^2} = \frac{2}{(\sin 3\theta)^2}\left\{g(\theta) - \frac{c(1+c)\left[(1+c^2)^2 - 5c(1-c^2)(1-c^2)\sin 3\theta\right]}{\sqrt{\left[(1+c^2)^2 + 4c(1-c^2)\sin 3\theta\right]^3}}\right\} \tag{A6}$$

DOI: 10.1002/nag

The expression for $\frac{\partial f}{\partial H}$ is

$$\frac{\partial f}{\partial H} = -e^{-k_h(A-1)^2} \tag{A7}$$

ACKNOWLEDGEMENTS

This work was supported by Research Grants Council of Hong Kong (GRF 622910 and SBI08/09.EG02). Y. F. Dafalias acknowledges funding from the European Research Council under the European Union's Seventh Framework Program (FP7/2007–2013) / ERC IDEAS Grant Agreement no 290963 (SOMEF) and partial support by NSF project CMMI-1162096.

REFERENCES

1. Azami A, Pietruszczak S, Guo P. Bearing capacity of shallow foundations in transversely isotropic granular media. *International Journal for Numerical and Analytical Methods* 2009; **34**(8): 771–793. DOI: 10.1002/nag.827.
2. Yamada Y, Ishihara K. Anisotropic deformation characteristics of sand under three-dimensional stress conditions. *Soils and Foundations* 1979; **19**(2):79–94.
3. Lam W-K, Tatsuoka F. Effects of initial anisotropic fabric and σ_2 on strength and deformation characteristics of sand. *Soils and Foundations* 1988; **28**(1):89–106.
4. Hight DW, Gens A, Symes MJ. The development of a new hollow cylinder appratus for investigating the effects of principal stress rotation in soils. *Geotechnique* 1983; **33**(4):355–383.
5. Yoshimine M, Ishihara K, Vargas W. Effects of principal stress direction and intermediate principal stress on undrained shear behaviour of sand. *Soils and Foundations* 1998; **38**(3):179–188.
6. Nakata Y, Hyodo M, Murata H, Yasufuku N. Flow deformation of sands subjected to principal stress rotation. *Soils and Foundations* 1998; **38**(2):115–128.
7. Uthayakumar M, Vaid YP. Static liquefaction of sands under multiaxial loading. *Canadian Geotechnical Journal* 1998; **35**:273–283.
8. Guo PJ. Modified direct shear test for anisotropic strength of sand. *Journal of Geotechnical and Geoenvironmental Engineering, ASCE* 2008; **134**(9):1311–1318.
9. Sekiguchi H, Ohta K. Induced anisotropy and time dependency in clays. In *Constitutive Equations of Soils*, *Proceedings of the 9th International Conference on Soil Mech. Found. Eng*., *Special Session 9*, Tokyo, 1977; 229–238.
10. Anandarajah A, Dafalias YF. Bounding surface plasticity, III: Application to anisotropic cohesive soils. *Journal of Engineering Mechanics, ASCE* 1986; **112**(12):1292–1318.
11. Pestana JM, Whittle AJ. Formulation of a unified constitutive model for clays and sands. *International Journal for Numerical and Analytical Methods in Geomechanics* 1999; **23**:1215–1243.
12. Hashiguchi K, Mase T. Extended yield condition of soils with tensile yield strength and rotational hardening. *International Journal of Plasticity* 2007; **23**:1939–1956.
13. Kaliakin VN. An assessment of the macroscopic quantification of anisotropy in cohesive soils. *Prco. 1st Japan-U.S. Workshop on Testing*, *Modeling*, *and Simulation*, *Boston*, *Massachusetts*, *USA*, 2003; 370–393.
14. Oda M, Nakayama H. Yield function for soil with anisotropic fabric. *Journal of Engineering Mechanics, ASCE* 1989; **115**(1):89–104.
15. Tobita Y, Yanagisawa E. Modified stress tensor for anisotropic behavior of granular materials. *Soils and Foundations* 1992; **32**(1):85–99.
16. Pietruszczak S. On inelastic behaviour of anisotropic frictional materials. *Mechanics of Cohesive-Frictional Materials* 1999; **4**:281–293.
17. Li XS, Dafalias YF. Constitutive modelling of inherently anisotropic sand behaviour. *Journal of Geotechnical and Geoenvironmental Engineering, ASCE* 2002; **128**(10):868–880.
18. Nemat-Nasser S, Zhang J. Constitutive relations for cohesionless frictional granular materials. *International Journal of Plasticity* 2002; **18**:531–547.
19. Dafalias YF, Papadimitriou AG, Li XS. Sand plasticity model accounting for inherent fabric anisotropy. *Journal of Engineering Mechanics, ASCE* 2004; **130**(11):1319–1333.
20. Zhu H, Mehrabadi MM, Massoudi M. Incorporating the effect of fabric in the dilatant double shearing model for planar deformation of granular materials. *International Journal of Plasticity* 2006a; **22**:628–653.
21. Zhu H, Mehrabadi MM, Massoudi M. Three-dimensional constitutive relations for granular materials based on the Dilatant Double Shearing mechanism and the concept of fabric. *International Journal of Plasticity* 2006b; **22**:826–857.
22. Anandarajah A. Multi-mechanism anisotropic model for granular materials. *International Journal of Plasticity* 2008; **24**:804–846.
23. Lashkari A, Latifi M. A non-coaxial constitutive model for sand deformation under rotation of principal stress axes. *International Journal for Numerical and Analytical Methods in Geomechanics* 2008; **32**(9):1051–1086.

24. Li XS, Dafalias YF. Anisotropic critical state theory: the role of fabric. *Journal of Engineering Mechanics, ASCE* 2012; **138**(3):263–275.
25. Rothenburg L, Bathurst RJ. Analytical study of induced anisotropy in idealized granular materials. *Geotechnique* 1989; **39**(4):601–614.
26. Kruyt NP, Rothenburg L. Kinematic and static assumptions for homogenization in micromechanics of granular materials. *Mechanics of Materials* 2004; **36**:1157–1173.
27. Thornton C, Zhang L. On the evolution of stress and microstructure during general 3D deviatoric straining of granular media. *Geotechnique* 2010; **60**(5):333–341.
28. Li XS, Li X. Micro–macro quantification of the internal structure of granular materials. *Journal of Engineering Mechanics, ASCE* 2009; **135**(7):641–656.
29. Guo N, Zhao J. The signature of shear-induced anisotropy in granular media. *Computers and Geotechnics* 2013; **47**:1–15.
30. Nicot F, Darve F. Basic features of plastic strains: from micro-mechanics to incrementally nonlinear model. *International Journal of Plasticity* 2007; **23**:1555–1588.
31. Verdugo R, Ishihara K. The steady state of sandy soils. *Soils and Foundations* 1996; **36**(2):81–91.
32. Nemat-Nasser S. A micromechanically-based constitutive model for frictional deformation of granular materials. *Journal of the Mechanics and Physics of Solids* 2000; **48**:1541–1563.
33. Li XS, Dafalias YF. A constitutive framework for anisotropic sand including non-proportional loading. *Geotechnique* 2004; **54**(1):41–55.
34. Jafarzadeh F, Javaheri H, Sadek T, Muir Wood D. Simulation of anisotropic deviatoric response of Hostun sand in true triaxial tests. *Computers and Geotechnics* 2008; **35**:703–718.
35. Li XS. Thermodynamics-based constitutive framework for unsaturated soils. 1: Theory. *Geotechnique* 2007; **57**(5):411–422.
36. Collins IF. The concept of stored plastic work or frozen elastic energy in soil mechanics. *Geotechnique* 2005; **55**(5):373–382.
37. Zhao J, Guo N. Unique critical state characteristics in granular media considering fabric anisotropy. *Géotechnique* 2013; **63**(8):695–704.
38. Zhao J, Guo N. A new definition on critical state of granular media accounting for fabric anisotropy. Powders and Grains 2013: Proceedings of the 7th International Conference on Micromechanics of Granular Media. 2013; **1542**: 229–232. DOI: http://dx.doi.org/10.1063/1.4811909
39. Richart FE Jr, Hall JR, Woods RD. *Vibrations of Soils and Foundations*. Prentice-Hall: Englewood Cliffs, NJ, 1970.
40. Li XS, Dafalias YF. Dilatancy for Cohesionless Soils. *Geotechnique* 2000; **50**(4):449–460.
41. Wang ZL, Dafalias YF, Shen C-K. Bounding surface hypoplasticity model for sand. *Journal of Engineering Mechanics, ASCE* 1990; **116**(5):983–1001.
42. Gutierrez M, Ishihara K, Towhata I. Model for the deformation of sand during rotation of principal stress directions. *Soils and Foundations* 1993; **33**(3):105–117.
43. Manzari MT, Dafalias YF. A two-surface critical plasticity model for sand. *Geotechnique* 1997; **47**(2):255–272.
44. Been K, Jefferies MG. A state parameter for sands. *Geotechnique* 1985; **35**(2):99–112.
45. Li XS, Wang Y. Linear representation of steady-state line for sand. *Journal of Geotechnical and Geoenvironmental Engineering* 1998; **124**(12):1215–1217.
46. Wan RG, Guo PJ. Effect of microstructure on undrained behaviour of sands. *Canadian Geotechnical Journal* 2001; **38**:16–28.
47. Fu P, Dafalias YF. Fabric Evolution within Shear Bands of Granular Materials and its Relation to Critical State Theory. *International Journal for Numerical and Analytical Methods in Geomechanics* 2011; **35**:1918–1948.
48. Oda M, Konishi J. Microscopic deformation mechanism of granular material in simple shear. *Soils and Foundations* 1974; **14**(4):25–38.
49. Dafalias YF. Plastic spin: Necessity or redundancy? *International Journal of Plasticity* 1998; **14**(9):909–931.
50. Chillarige AV, Robertson PK, Morgenstern NR, Christian HA. Evaluation of the in situ state of Fraser River sand. *Canadian Geotechnical Journal* 1997; **34**:510–519.
51. Taiebat M, Dafalias YF. SANISAND: Simple anisotropic sand plasticity model. *International Journal for Numerical and Analytical Methods in Geomechanics* 2008; **32**(8):915–948.
52. Papadimitriou AG, Dafalias YF, Yoshimine M. Plasticity modeling of the effect of sample preparation method on sand response. *Soils and Foundations* 2005; **40**(2):109–124.
53. Li X, Yu HS. Numerical investigation of granular material behavior under rotational shear. *Geotechnique* 2010; **60**(5):381–394.
54. Li X. Micro-scale investigation on the quasi-static behavior of granular material. PhD thesis, Hong Kong University of Science and Technology, 2006.

DOI: 10.1002/nag